



Exploring NiO nanosize structures for ammonia sensing

M. M. Gomaa^{1,2} · G. RezaYazdi² · M. Rodner² · G. Greczynski² · M. Boshta¹ · M. B. S. Osman³ · V. Khranovskyy² · J. Eriksson² · R. Yakimova²

Received: 16 January 2018 / Accepted: 11 May 2018 / Published online: 21 May 2018
© The Author(s) 2018

Abstract

Efficient ammonia gas sensor devices were fabricated based on nickel oxide (NiO) nanostructures films. Two chemical synthesis approaches were used: chemical spray pyrolysis (CSP) and chemical bath deposition (CBD), aiming at obtaining highly developed surface area and high chemical reactivity of NiO. Crystal structure, morphology, and composition of NiO films and nanostructures were investigated by scanning electron microscopy, X-ray diffraction, and X-ray photoelectron spectroscopy. CSP method results in the synthesis of NiO films with pure cubic crystalline structure of preferred orientation along (111) direction. The type of the precursors used (nickel acetate, nickel chloride and nickel nitrate) affects the morphology and crystallites average size of the deposited films. CBD method consisted of two stages: (i) deposition of nickel hydroxide phase and (ii) thermal annealing of nickel hydroxide at 450 °C in air for 4 h. Resulted structures were nanoflakes, vertically arranged in a “wall-like” morphology. Fabricated structures were found to be sensitive to ammonia differently, depending on the synthesis approach and material morphology. NiO films deposited by CBD demonstrated a stable response to ammonia with maximum magnitude at the operating temperature of 300 °C. The highest average response for the CBD–NiO sample was 114.3–141.3% for 25 and 150 ppm NH₃, respectively, whereas the response range observed for the film processed by spray pyrolysis using nickel chloride was 31.7–142.5% for 25 and 150 ppm NH₃, respectively.

1 Introduction

Growing needs in gas sensors applications in agricultural processes, industrial emission control, environmental monitoring and disease diagnostic [1, 2] have motivated a constant search for new ambience sensitive materials. This can be satisfied either via synthesis of novel chemically active materials or enhancement of materials sensitivity by decreasing their dimensions, or both [3]. Metal oxide semiconductors are considered appropriate gas sensing materials due to the sensitivity of their stoichiometry to the ambience gas composition, resulting in a stable and reproducible change of their electronic properties upon the change of the gas concentrations near the surface of the materials [4–7].

Nickel oxide (NiO) is a prospective *p*-type metal oxide semiconductor with such sensing-desirable properties as high melting point (1960 °C), high chemical stability and wide direct energy gap (3.6–4.0 eV) [8]. The electrical conductivity of NiO films can be varied by the change of Ni vacancies and/or interstitial oxygen in the NiO structure [9, 10]. The change of NiO features is due to their nonstoichiometric effect that makes the films suitable for many applications like solar cells [11, 12], electrochromic applications [13–16], optoelectronic applications based on *p*-*n* junctions such as UV detectors and LEDs [17, 18]. Earlier, it was reported that NiO thin films can sense reducing gases such as NH₃, CH₄, and H₂ [19–21] as well as oxidizing gases like NO₂ [22]. Particularly, detection of ammonia is essential for such industries as agriculture, food and beverages or fertilizer production. The main artificial ammonia sources in the air come from intensive livestock with the decomposition process of manure, as well as the production of fertilizers and refrigeration systems by the chemical industry. The toxicity threshold limit value (TLV) for NH₃ gas is 25 ppm [23], which makes the detection of ammonia in the atmosphere very important due to the hazard implications on the environment [24].

✉ M. M. Gomaa
mohme00@ifm.liu.se; dr.metwalyg@gmail.com

¹ Solid State Physics Department, National Research Centre, El-Behouth st., Dokki 12622, Giza, Egypt

² Department of Physics, Chemistry and Biology, Linköping University, 58183 Linköping, Sweden

³ Physics Department, Faculty of Girls, Ain Shams University, Heliopolis, Cairo, Egypt

NiO has been synthesized as films and nanostructures by various physical and chemical deposition techniques, such as sputtering [25], electron beam evaporation [15], sol–gel [26], pulsed laser deposition [27], chemical bath deposition [28] and chemical spray pyrolysis [29]. Among others, chemical spray pyrolysis (CSP) and chemical bath deposition (CBD) are most economically viable techniques, allowing fabrication of homogeneous oxide material on large-area substrates at a relatively low deposition temperature [28]. Nevertheless, obtaining a proper NiO material with necessary characteristics for advanced gas sensing is still an issue: while dense films deposited on solid substrates are robust and convenient for contacting, their surface area is rather limited, thus decreasing the sensitivity. On the other hand, dispersed NiO nanostructures have high surface area and thus high sensitivity but are difficult to be contacted for practical use. Therefore, controlled fabrication of NiO nanostructures with high surface area on desired substrates is presently a challenge.

In this work, we have compared CSP and CBD techniques for growth of NiO material on glass substrates, varying the material morphology and surface area and aiming at advanced ammonia sensing properties. Crystal structure, morphology, and composition of NiO were characterized by XRD, SEM, and XPS, respectively. It was observed, that CSP results in NiO thin films, sensitive to ammonia, with high response. While CBD, conducted in two stages—via deposition of nickel hydroxide phase and its thermal annealing—resulted in a vertically arranged “wall-like” morphology, consisting of nanoflakes structure. The CBD fabricated structure was found to be extremely sensitive to the lowest amount of ammonia tested (25 ppm), providing 114.3% of the sensor response.

2 Experimental details

2.1 Samples fabrication

Nickel oxide films were synthesized by chemical spray pyrolysis approach (CSP) using 0.2 M aqueous solution of nickel precursors; nickel acetate, nickel chloride and nickel nitrate. Before deposition process, the glass substrate was cleaned chemically and ultrasonically using acetone in an ultrasonic bath for 20 min, deionized water and alcohol; successively. In order to obtain highly controlled and uniform films, the starting solution was sprayed to very fine droplets using automatic Spray Gun HM-3 atomizer onto the heated glass substrate at 450 °C. The deposition time, the pressure of the compressed air and the distance between the nozzle and the substrate were kept constant for all NiO films deposited using different precursor at 10 min, 1.5 bar and

30 cm, respectively. A detailed description of chemical spray pyrolysis method can be found elsewhere [29].

Nickel chloride was used as a precursor for the deposition of NiO nanostructure on glass substrates using chemical bath deposition method (CBD). The substrates were carefully cleaned as in the previous technique. The optimum temperature during the deposition process was 50 ± 2 °C and the pH value was 12. The as-deposited film was nickel hydroxide which transformed to nickel oxide with annealing in air at 450 °C for 4 h. A detailed description of the CBD method and the reaction mechanism for deposition of NiO nanostructures can be found elsewhere [28].

2.2 Material characterization

The crystallographic structure of nickel oxide and nickel hydroxide films was examined by X-ray diffraction (XRD) measurements with a Panalytical X'Pert diffractometer using (Cu K α radiation at 45 kV and 40 mA). Scanning electron microscopy (SEM) was performed to study surface morphology of deposited films before gas measurements as well as after introducing ammonia gas using Leo 1550 Gemini microscope at an operating voltage of 10 kV. Dektak 150 Stylus profilometer was used to measure the thickness of deposited films. The chemical composition of the films was analyzed by X-ray photoelectron spectroscopy (XPS) using Axis Ultra DLD instrument from Kratos Analytical, (Manchester, UK) to study the change of chemical composition as well as bonding states of NiO films after gas sensing measurements. XPS core level spectra of Ni 2p, C 1s, and O 1s regions were acquired after sputter cleaning for 600 s with a 500 eV Ar⁺ beam incident at 70° angle from surface normal. Binding energy referencing was performed according to the procedure described by Greczynski et al. [30].

2.3 Sensors fabrication

Sensor devices have been fabricated on glass substrates with two squared electrodes on top of the NiO films through evaporating titanium (2 nm) and gold (200 nm) sequentially. The electrodes are 2 mm wide with a 1 mm gap in between. To enable a controlled temperature loop, each sensor chip is glued using Aremco Ceramabond 571 on top of a ceramic heater substrate (Heraeus GmbH, Germany) with an additional Pt-100 temperature sensor (Heraeus GmbH, Germany). This device was mounted on top of a TO8-socket and connected to its pins using gold-wire bonding and silver glue (Epotek E3081). This setup limits the temperature that can be used within stable conditions to 300 °C. The final sensor is inserted into a flow cell which is attached to a gas mixing system. A brief description of this system can be found elsewhere [31]. The dry background mixture of N₂ and O₂ with a ratio of 80:20 ml/min and a constant flow rate of 100 ml/min

was used both as a carrier gas and purging gas. The nitrogen concentration was then adjusted when introducing ammonia to the gas flow. Each test gas exposure lasted for 15 min with a 45-min background gas exposure for recovery and was repeated twice before a new concentration was introduced.

3 Results and discussion

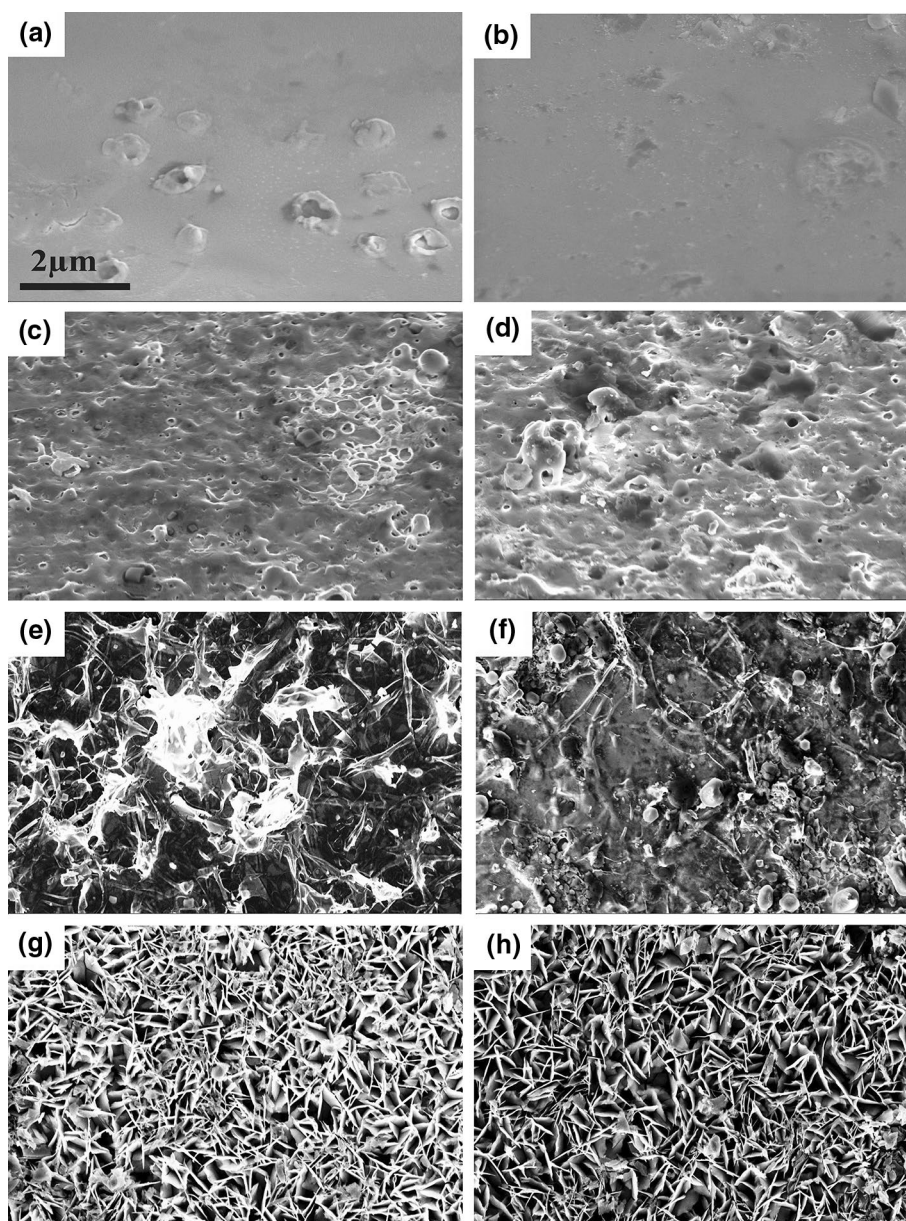
3.1 Surface morphology

SEM images of NiO films and nanostructures obtained by both CSP and CBD methods are presented in Fig. 1a, c, e, g. Furthermore, we have studied the structure of NiO films also after the ammonia sensing measurements (Fig. 1b,

d, f, h). The surface of CSP–NiO film based on nickel acetate has an anomalous shape and the surface of film based on nickel chloride has a holes, which increase the surface roughness of the films. It is also seen that the surface morphology of CSP–NiO using nickel acetate has changed after ammonia exposure which has an effect on the stability of the sensor response as well (will be shown later). In contrast, the sprayed CSP–NiO using nickel nitrate presents a smooth grainy surface and no significant change in the surface morphology can be seen after gas measurements.

The CBD–NiO film exhibits a different morphology: nanoflakes—of NiO are vertically arranged into a “wall-like” microstructure (Fig. 1g). We attribute such specific structure of nanoflakes to the type of the precursor used, as

Fig. 1 SEM micrographs of CSP–NiO films using different precursors; **a** chloride, **c** acetate, **e** nitrate and **g** CBD–NiO nanoflakes before gas sensing and **b**, **d**, **f**, **h** after gas sensing measurements of the corresponding films. The scale in the image **a** is valid for all images



well as the post-deposition annealing. Apparently, the nanoflakes are crystallized from nickel hydroxide matrix during annealing phase. It has to be noticed, that the nanostructures were not affected by ammonia sensing response, unlike the CSP NiO films (see above), and are structurally stable and robust after repetitive sensing measurements at 300 °C (Fig. 1h). The nanoflakes structure contributes significantly to the active surface area and therefore was expected to have a superior sensing performance.

3.2 Structural properties

Figure 2 shows the θ - 2θ scans of the NiO films and nanostructure deposited by CSP and CBD techniques. It can be clearly seen that the broad peak located at $2\theta=24$ is assigned to the amorphous glass substrate. The sprayed NiO using nickel chloride and nickel nitrate exhibit high peak intensities, while the NiO film prepared using nickel acetate has lower intensities. Furthermore, peak position and phase identification analysis show that all diffraction peaks belong to NiO with cubic structure (pdf no. 047 1049) with a predominant 111-preferred

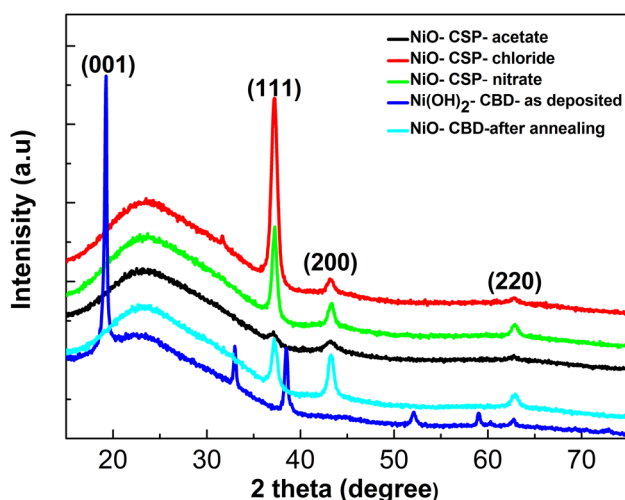


Fig. 2 X-ray diffraction θ - 2θ scan of CSP-NiO using different precursor and CBD-NiO films (both as-deposited nickel hydroxide and NiO after annealing at 450 °C for 4 h)

orientation [29]. Otherwise, the diffraction patterns of the as-deposited film by CBD is corresponding to nickel hydroxide Ni(OH)₂ phase (pdf no: 74-2075) with high peak intensity at 2θ position 19.2° which indexed as (001) plane. The annealed film at 450 °C in air for 4 h shows that all diffraction peaks correspond to cubic NiO (pdf no. 047 1049). The diffraction peaks of NiO films prepared by CSP and CBD methods have been labeled with the corresponding Miller indices. In addition, the d spacing and lattice constant were calculated from the peak position. The crystallite size of deposited films was calculated using the Debye Scherrer formula for the (111) diffraction peaks. The CSP-NiO using nickel chloride has the largest crystallite size, whereas the CSP-NiO using nickel acetate has the smallest crystallite size. These results can be found in Table 1.

3.3 Gas sensing properties

The working temperature is one of the main parameters that determine the response of a gas sensor, since it controls the processes of adsorption and desorption of the different gas species existing in the surrounding atmosphere on the surface [4]. First, we have studied the temperature dependence of CSP-NiO films sensitivity to 150 ppm ammonia concentration at different operating temperatures (Fig. 3a). With an increase of the operating temperature, the response increases from 6.6% at 100 °C until it reaches its maximum of 99.7% at 300 °C. The temperature 300 °C was then used as the operating point for all further measurements with different ammonia concentrations.

Figure 3b shows the dynamic resistance of a sensor for different ammonia concentrations (25, 50, 100 and 150 ppm) at 300 °C operating temperature. It can be clearly seen that the resistance of the NiO increases for all four sensors when ammonia gas is introduced into the measurement system. This is due to the interaction of ammonia with adsorbed oxygen on the surface of the NiO films, resulting in the production of H₂O vapor and free electrons. The free electrons recombine with holes, which are the majority charge carriers in NiO. Therefore, the reduction in the number of holes results in an increase of resistance.

Table 1 Structural parameters of NiO films and nanostructures, prepared by CSP and CBD methods

Method	NiO precursors	Thickness t (nm)	2 theta	$d_{(111)}$	Lattice constant a (nm)	Crystallite size D_{111} (nm)
Chemical spray pyrolysis (CSP)	Nickel acetate	275	37.141	2.419	0.419	10
	Nickel chloride	300	37.197	2.415	0.418	57
	Nickel nitrate	270	37.213	2.414	0.418	25
Chemical bath deposition (CBD)	Nickel chloride	340	37.198	2.415	0.418	20

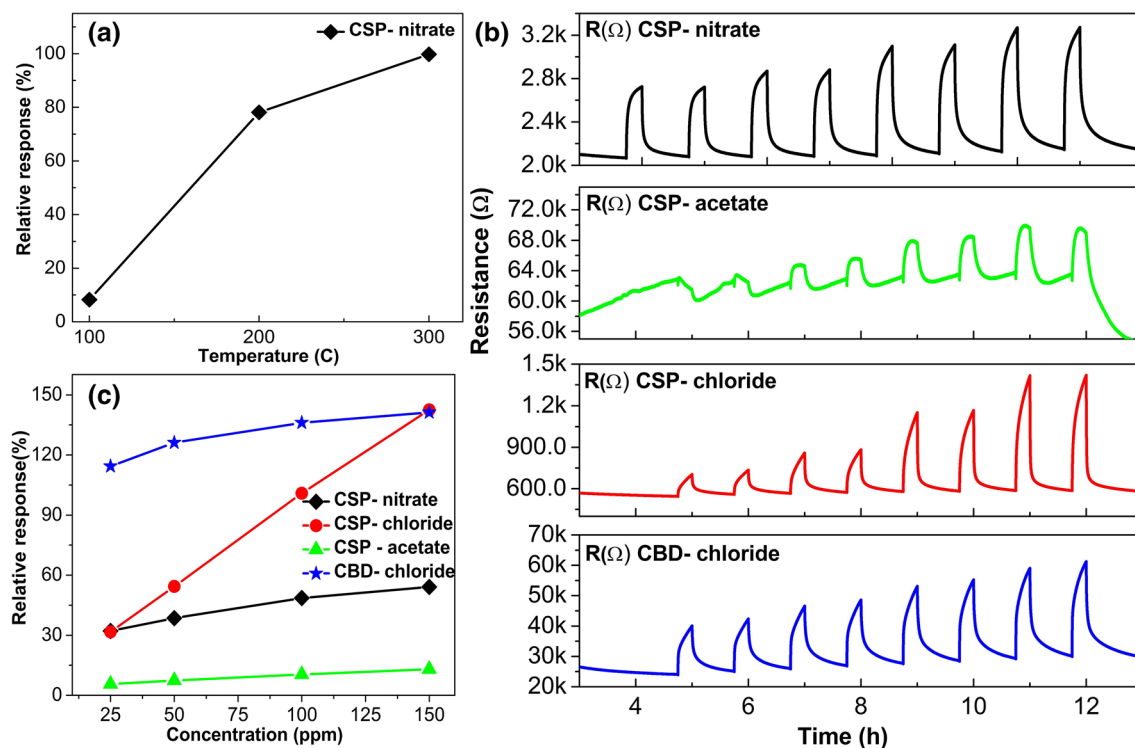
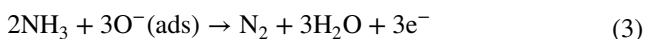


Fig. 3 **a** Sensor response at different operating temperatures for 150 ppm NH₃, **b** raw sensor signal for 25, 50, 100 and 150 ppm of NH₃ at 300 °C for the different processed materials and **c** relative sensor response comparison for the different materials towards NH₃

The reaction summary for ammonia gas in this study is listed below [24]:



In addition, the sensing response of NiO depends on different factors such as surface morphology, crystallite size, surface states and adsorption efficiency of target gas molecules on the surface as well as the reaction with adsorbed oxygen or lattice oxygen [24].

The relative response, S , is defined as the ratio of the sensor baseline resistance in background gas and the highest sensor resistance recorded after introducing the target gas and is calculated according to Eq. (4) [32]:

$$S = \frac{R_{\text{gas}} - R_{\text{background}}}{R_{\text{background}}} \times 100\% \quad (4)$$

The calculated response values are reported in Fig. 3c as a function of ammonia concentration. It can be clearly seen that the response significantly depends on the preparation conditions which affect the surface morphology, the degree of crystallinity as well as the chemical composition

of the NiO films. The best dynamic response is obtained for CSP–NiO using nickel chloride with a response of 31.7% for 25 ppm to 142.5% for 150 ppm, respectively. This behavior could be attributed to the high surface roughness, which increases the active surface area resulting in an increase of the adsorption sites available for gas interaction. The response of CSP–NiO sensor using nickel nitrate has demonstrated a medium dynamic response of 32% for 25 ppm to 54% for 150 ppm, respectively. This decrease in sensitivity might be explained by the lower surface roughness, thus decreasing possible adsorption sites. Although the CSP–NiO sensor prepared using nickel acetate has irregular rings which increase the surface roughness, it exhibits the lowest response for all concentrations with a change in resistance of 5.6% for 25 ppm and 13% for 150 ppm, respectively. This could be explained by this film having the lowest crystallite size and a very unstable surface.

The *highest average response* was found for the nanostructures of NiO deposited by CBD: with 114.3–141.3% for 25 and 150 ppm of NH₃, respectively, and can be directly linked to the large surface area of the nanostructures. The ammonia sensitivity of our nanostructures for this concentration range is roughly 20 times higher than that of a recently reported ammonia sensor based on NiO films [33]. In addition, the CBD–NiO sensor has an average t_{90} time constants

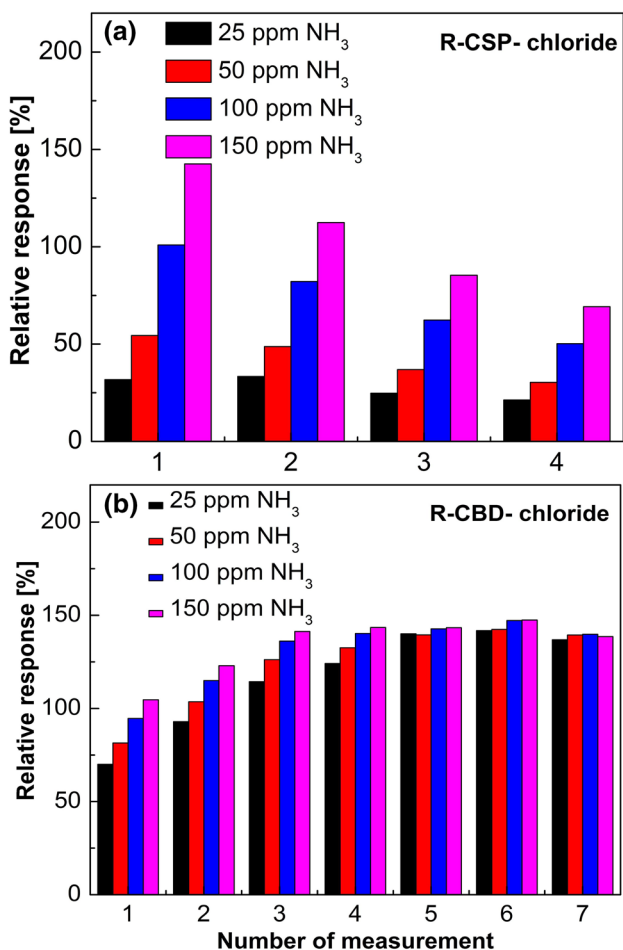


Fig. 4 Sensor response upon repeated exposure to different NH₃ concentrations of (a) CSP–NiO using nickel chloride and (b) CBD–NiO nanostructure

of 650 s which make it faster than the CSP–NiO using nickel chloride which has an average of 740 s.

Besides the plain response over concentration measurements, also the response over several measurement cycles was tested to see if the sensors show a stable and reproducible response.

Figure 4 shows the dynamic sensing performance of two selected sensors both prepared using nickel chloride over several sensing cycles. The CSP–NiO sensor exhibits a high dynamic response with increasing ammonia concentration in the same sensing cycle but, overall sensor performance decreases over several sensing cycles.

On the contrary, the response performance of the sensor based on CBD–NiO nanostructures increases for the first four sensing cycles until it reaches its maximum and then levels out all responses, even for different concentrations to the same level. Interestingly, the sensor maintains a repeatable and high response (over 110%) for minimal ammonia concentration (25 ppm), while negligible or no difference in signal is observed with further ammonia concentration increase. Such a behavior can be useful in specific applications, for the “caution” detection of ammonia, providing a warning to the customers. We explain this behavior as following: the gas sensor performance is affected by the chemical composition and chemisorbed oxygen species on the sensing surface [34]. Additionally, the relative amount of nickel vacancy in the nickel oxide is also responsible for signal providing [34]. Nanostructures of NiO, deposited by CBD, are in fact tiny single crystals and are of high structural quality. Due to their structure and exposure of the major part of the material to the ambience, the process of electron trapping is rather fast and saturates already at the lowest ammonia concentration, providing a high and stable signal, while further increase of ammonia content does

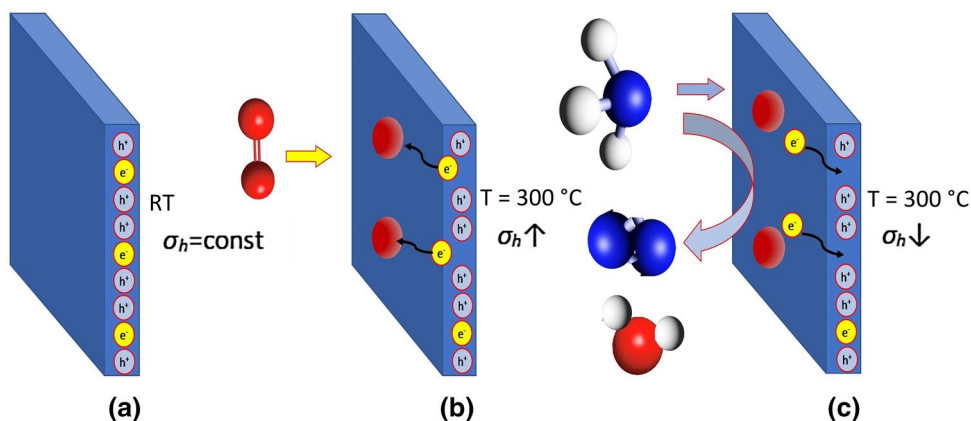


Fig. 5 Ammonia sensitivity mechanism for the case of CBD–NiO nanostructures: **a** at room temperature NiO possesses hole conductivity with minor electron concentration; **b** at operating temperature 300 °C oxygen molecules are adsorbed on the NiO surface (see formula 1) and dissociated into oxygen ions (see formula 2), removing

electrons and thus increasing hole conductivity; **c** ammonia molecules are adsorbed on the NiO surface and dissociated into nitrogen and hydrogen ions, later associating into nitrogen gas and water, simultaneously providing electrons back and decreasing the conductivity of NiO

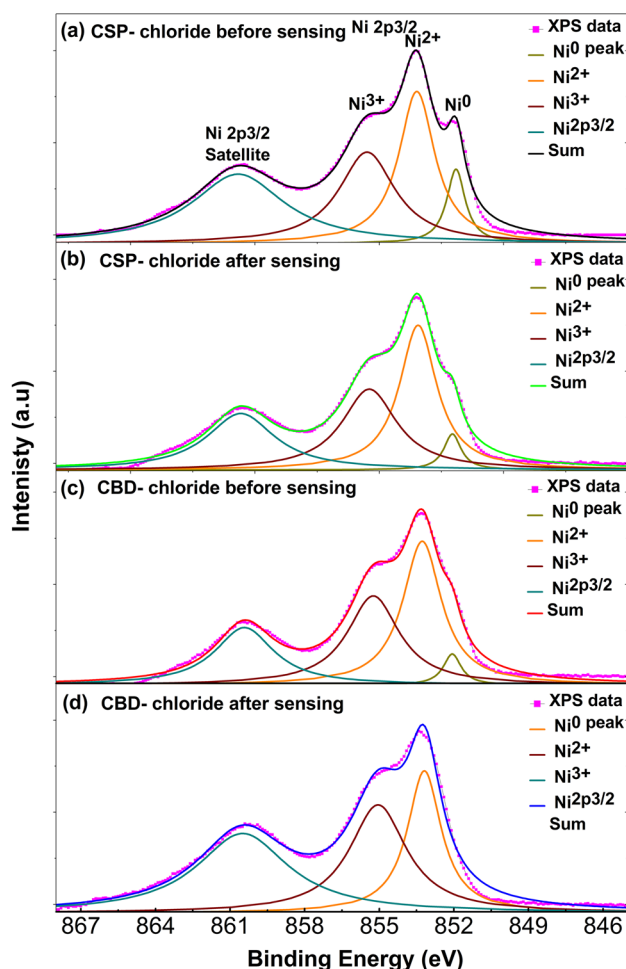


Fig. 6 Ni $2p_{3/2}$ XPS core level spectra obtained from NiO thin films and nanostructures, prepared by CSP (a, b) and CBD (c, d)

not lead to any further reaction. We present a schematic, describing ammonia sensing mechanism, particularly for the case of CBD–NiO nanostructures (Fig. 5).

We have performed XPS measurements to study the effect of chemical composition and bonding states contribution of NiO films and nanostructure on the sensing performance. Figure 6a–d shows the Ni $2p_{3/2}$ core level spectra of the sprayed NiO films using nickel chloride. The proposed deconvolution includes three peaks, the main peak can be assigned to Ni²⁺ with the binding energy of 853.4 eV and the shoulder peaks attributed to Ni⁰, and Ni³⁺ with binding energies of 852 and 855.1 eV, respectively. The bonding state Ni³⁺ can be created by negatively charged oxygen on the surface of NiO and/or by negatively charged interstitial oxygen [34]. The Ni $2p_{3/2}$ spectra obtained from the NiO films after sensing measurements show a decrease in the Ni⁰ component and an increase in the amount of Ni³⁺ due to oxidation, which leads to supplement of the conductivity of NiO films due to the increase of the hole creation [29].

The created holes decrease the resistance of the sensor after each sensing cycle which fits the observed degradation of sensor response in Fig 4a.

The deconvolution of Ni $2p_{3/2}$ core level spectra for CBD–NiO films using nickel chloride (see Fig. 6c, d). The deconvoluted peaks have binding energies of 852.2, 853.4 and 855.2 eV, corresponding to Ni⁰, Ni²⁺, and Ni³⁺, respectively. Compared to the sprayed NiO films, the Ni³⁺ component is larger, while the Ni⁰ component is smaller. The steady response of the CBD–NiO sensor for different ammonia concentrations after the fourth cycle may be attributed to the complete disappearance of Ni⁰ peaks and a small increase in the Ni³⁺ peak. Moreover, the sensitivity might decrease as a result of the slightly reduced specific area due to temperature effects [35].

4 Conclusion

Ammonia gas sensors based on NiO were successfully fabricated using NiO films and nanostructures prepared by spray pyrolysis and chemical bath deposition. Sprayed NiO films using nickel chloride and nickel acetate exhibit uneven surfaces which increased roughness of deposited films while the films prepared using nickel nitrate have a smooth surface. Chemical bath deposition approach carried out in two steps—via deposition of nickel hydroxide phase and its thermal annealing—resulted in a vertically arranged “wall-like” morphology, consisting of nanoflakes structure, which increases the surface area as well as enhances the gas sensor response. The XRD studies show all CSP–NiO films using nickel acetate, nickel chloride and nickel nitrate have a cubic poly-crystalline structure with a preferred orientation along (111) direction. While the as-deposited films using chemical bath deposition are nickel hydroxide phase which transformed to poly-crystalline NiO phase by an annealing process. The different NiO materials show distinct differences in their sensor response, depending on the surface morphology and chemical composition. The XPS results confirm that the changes in the sensor behavior depends on the chemical composition of NiO films consequently the Ni/O ratio of different precursors. The highest average response was found for the CBD–NiO film, which also has the highest surface area due to its nanoflakes structure, whereas the highest dynamic range belonged to the CSP–NiO using nickel chloride. Besides the very good response and dynamic range, the main drawback is the stability with a decrease in response for the CSP sensors based on nickel chloride. The CBD–NiO nanostructure was found to be extremely sensitive to the lowest amount of ammonia tested, with a repeatable high signal intensity providing 114.3% of the sensor response, while negligible or no difference in signal is observed with

further ammonia concentration increase. This behavior can be useful for the “caution” detection of ammonia, providing warning signals to the customers.

Acknowledgements The authors acknowledge the financial support by the Egyptian Ministry for Higher Education and Scientific Research, Collaborative Research Project between Egypt and Sweden funded by the Swedish Research Council (VR 348-2013-6782), and Ångpanneföreningens Forskningsstiftelse (Grant 14-517) and Swedish Research Council (VR) Marie Skłodowska Curie International Career Grant #2015-00679 “GREEN 2D FOX”.

Open Access This article is distributed under the terms of the Creative Commons Attribution 4.0 International License (<http://creativecommons.org/licenses/by/4.0/>), which permits unrestricted use, distribution, and reproduction in any medium, provided you give appropriate credit to the original author(s) and the source, provide a link to the Creative Commons license, and indicate if changes were made.

References

1. A.I. Ayesh, J. Nanomater. **2016**, 2359019 (2016). <https://doi.org/10.1155/2016/2359019>
2. Y. Shon, H. Kim, H.S. Hwang, E.S. Bae, T. Eom, E.J. Park, W.-S. Ahn, J.J. Wie, B.S. Shim, Sens. Actuators B **244**, 1–10 (2017)
3. Y.-F. Sun, S.-B. Liu, F.-L. Meng, J.-Y. Liu, Z. Jin, L.-T. Kong, J.-H. Liu, Sensors (Basel) **12**(3), 2610–2631 (2012)
4. N. Barsan, U. Weimar, *IMCS 2012 the 14th International Meeting on Chemical Sensors* (Wunstorf AMA Service GmbH, Nuremberg, 2012), pp. 618–621
5. J. Zhang, Z. Qin, D. Zeng, C. Xie, Phys. Chem. Chem. Phys. **19**, 6313–6329 (2017)
6. C. Wang, L. Yin, L. Zhang, D. Xiang, R. Gao, Sensors **10**, 2088–2106 (2010)
7. K. Sahner, H.L. Tuller, J. Electroceram. **24**(3), 177–199 (2010)
8. M. Jlassi, I. Sta, M. Hajji, H. Ezzaouia, Appl. Surf. Sci. **308**, 199–205 (2014)
9. Y.-M. Lee, C.-H. Hsu, H.-W. Chen, Appl. Surf. Sci. **255**(8), 4658–4663 (2009)
10. S. Kim, D. Chul, H. Lee, J. Appl. Phys. **112**, 3 (2012)
11. X. Xu, Z. Liu, Z. Zuo, M. Zhang, Z. Zhao, Y. Shen, H. Zhou, Q. Chen, Y. Yang, M. Wang, Nano Lett. **15**(4), 2402–2408 (2015)
12. J. He, H. Lindström, A. Hagfeldt, S.-E. Lindquist, J. Phys. Chem. B **103**(42), 8940–8943 (1999)
13. H. Moulki, C. Faure, M. Mihelcic, A.S. Vuk, F. Svegl, B. Orel, G. Campet, M. Alfredsson, A.V. Chadwick, D. Gianolio, A. Rougier, Thin Solid Films **553**, 63–66 (2014)
14. D.R. Sahu, T. Wu, S. Wang, J. Huang, J. Sci. Adv. Mater. Devices **2**(2), 225–232 (2017)
15. S. Pereira, A. Goncalves, N. Correia, J. Pinto, L. Pereira, R. Martins, E. Fortunato, Sol Energy Mater. Sol Cells **120**, 109–115 (2014)
16. G.F. Cai, C.D. Gu, J. Zhang, P.C. Liu, X.L. Wang, Y.H. You, J.P. Tu, Electrochim. Acta **87**, 341–347 (2013)
17. A. Echresh, C.O. Chey, M. Zargar Shoushtari, V. Khranovskyy, O. Nur, M. Willander, J. Alloys Compd. **632**, 165–171 (2015)
18. H. Wang, Y. Zhao, C. Wu, G. Wu, Y. Ma, X. Dong, B. Zhang, G. Du, Opt. Commun. **395–397**, 94 (2017)
19. P.C. Chou, H.I. Chen, I.P. Liu, C.C. Chen, J.K. Liou, K.S. Hsu, W.C. Liu, IEEE Sens. J. **15**(7), 3711–3715 (2015)
20. H. Steinebach, S. Kannan, L. Rieth, F. Solzbacher, Sens. Actuators B **151**(1), 162–168 (2010)
21. A.M. Soleimanpour, A.H. Jayatissa, G. Sumanasekera, Appl. Surf. Sci. **276**, 291–297 (2013)
22. I. Hotovy, V. Rehacek, P. Siciliano, S. Capone, L. Spiess, Thin Solid Films **418**(1), 9–15 (2002)
23. W. Olthuis, A. Van Den Berg, Sens. Actuators B **107**, 666–677 (2005)
24. C.S. Rout, M. Hegde, A. Govindaraj, Nanotechnology **18**, 20 (2007)
25. M. Guziewicz, J. Grochowski, M. Borysiewicz, E. Kaminska, J.Z. Domagala, W. Rzdokiewicz, B.S. Witkowski, K. Golaszewska, R. Kruzka, M. Ekielski, A. Piotrowska, Opt. Appl. **XLI**, 431–440 (2011)
26. I. Sta, M. Jlassi, M. Kandyla, M. Hajji, P. Koralli, R. Allagui, M. Kompitsas, J. Alloys Compd. **626**, 87 (2015)
27. M. Stamataki, D. Tsamakis, N. Brilis, I. Fasaki, A. Giannoudakos, M. Kompitsas, Phys. Stat. Sol. A **205**(8) 2064–2068 (2008)
28. M.M. Gomaa, M. Boshta, B.S. Farag, M.B.S. Osman, J. Mater. Sci. Mater. Electron. **27**(1), 711–717 (2016)
29. M.M. Gomaa, G.R. Yazdi, S. Schmidt, M. Boshta, V. Khranovskyy, F. Eriksson, B.S. Farag, M.B.S. Osman, R. Yakimova, Mater. Sci. Semicond. Process. **64**, 32–38 (2017)
30. G. Greczynski, L. Hultman, ChemPhysChem **18**(12), 1507–1512 (2017)
31. A.L. Spetz, M. Andersson, *Solid State Gas Sensors: Industrial Application. Chemical Sensors and Biosensors (Methods and Applications)*, vol. 11 (Springer, Berlin, 2011)
32. A.M. Soleimanpour, Y. Hou, A.H. Jayatissa, Appl. Surf. Sci. **257**(12), 5398–5402 (2011)
33. H.-I. Chen, C.-Y. Hsiao, W.-C. Chen, C.-H. Chang, T.-C. Chou, I.-Ping Liu, K.-W. Lin, W.-C. Liu, Sens. Actuators B **256**, 962–967 (2018)
34. C. Wang, X. Cui, J. Liu, X. Zhou, X. Cheng, P. Xiaolong, S. Xiaowei, H. Li, J. Zheng, G. Lu, ACS Sens. **1**(2), 131–136 (2016)
35. J. Zhang, D. Zeng, Q. Zhu, J. Wu, Q. Huang, C. Xie, J. Phys. Chem. C **120**(7), 3936–3945 (2016)